

Observable Gravitational Waves in Minimal Scotogenic Model

Debasish Borah,^{1,*} Arnab Dasgupta,^{2,†} Kohei

Fujikura,^{3,‡} Sin Kyu Kang,^{4,§} and Devabrat Mahanta^{1,¶}

¹*Department of Physics, Indian Institute of Technology Guwahati, Assam 781039, India*

²*Institute of Convergence Fundamental Studies , Seoul-Tech, Seoul 139-743, Korea*

³*Department of Physics, Tokyo Institute of Technology,*

2-12-1 Ookayama, Meguro-ku, Tokyo 152- 8551, Japan

⁴*School of Liberal Arts, Seoul-Tech, Seoul 139-743, Korea*

Abstract

We scrutinise the widely studied minimal scotogenic model of dark matter (DM) and radiative neutrino mass from the requirement of a strong first order electroweak phase transition (EWPT) and observable gravitational waves at future planned space based experiments. The scalar DM scenario is similar to inert scalar doublet extension of standard model where a strong first order EWPT favours a portion of the low mass regime of DM which is disfavoured by the latest direct detection bounds. In the fermion DM scenario, we get newer region of parameter space which favours strong first order EWPT as the restriction on mass ordering within inert scalar doublet gets relaxed. While such leptophilic fermion DM remains safe from stringent direct detection bounds, newly allowed low mass regime of charged scalar can leave tantalising signatures at colliders and can also induce charged lepton flavour violation within reach of future experiments. While we get such new region of parameter space satisfying DM relic, strong first order EWPT with detectable gravitational waves, light neutrino mass and other relevant constraints, we also improve upon previous analysis in similar model by incorporating appropriate resummation effects in effective finite temperature potential.

* dborah@iitg.ac.in

† arnabdasgupta@protonmail.ch

‡ fuji@th.phys.titech.ac.jp

§ skkang@seoultech.ac.kr

¶ devab176121007@iitg.ac.in

I. INTRODUCTION

The scotogenic framework, proposed by Ma in 2006 [1] has been one of the most popular extensions of the standard model (SM) which simultaneously account for the origin of light neutrino mass and dark matter (DM). In spite of significant experimental evidences confirming the non-vanishing yet tiny neutrino masses and the presence of a mysterious, non-luminous, non-baryonic form of matter, dubbed as DM [2], its origin remains unaddressed in the SM. While the latest experimental constraints on light neutrino parameters can be obtained from recent global fits [3, 4], the present DM abundance is quantified in terms of density parameter Ω_{DM} and $h = \text{Hubble Parameter (H)}/(100 \text{ km s}^{-1}\text{Mpc}^{-1})$ as [5]: $\Omega_{\text{DM}}h^2 = 0.120 \pm 0.001$ at 68% CL. The possibility of scalar DM in this model has been already studied in several works including [6–20], whereas that of thermal or non-thermal fermion DM has also been studied [21, 22]. The model can also account for the observed baryon asymmetry through successful leptogenesis (for a review of leptogenesis, see [23]) in variety of different ways [20, 22, 24–28]. While the observational evidences suggesting the presence of DM are purely based on its gravitational interactions, most of the particle DM models (including the scotogenic model) adopt a weak portal (but much stronger than gravitational coupling) between DM and the visible matter or the SM particles. If DM is of thermal nature, like in the weakly interacting massive particle (WIMP) paradigm (see [29] for a recent review), then such DM-SM couplings can be as large as the electroweak couplings and hence such DM can leave imprint on direct search experiments. However, none of the direct detection experiments like LUX [30], PandaX-II [31, 32] and Xenon1T [33, 34] have reported any positive signal yet, giving more and more stringent upper bounds on DM-nucleon interactions.

Although the ongoing direct detection experiments have not exhausted all parameter space yet, specially in the context of the minimal scotogenic model, it is equally important to look for complementary probes. Scalar DM in this model is not only tightly constrained by direct detection experiments mentioned above, but can also be probed at indirect detection experiments looking for excess in gamma rays [19] or X-rays [35] depending upon the particular DM candidate chosen. Apart from usual collider signatures of the scalar doublet like dijet or dileptons plus missing energy [14, 36–40], the scotogenic model can also give rise to exotic signatures like displaced vertex and disappearing or long-lived charged track

for compressed mass spectrum of inert scalars and singlet fermion DM [41]. Apart from collider signatures of inert scalars in the model, as discussed in several earlier works mentioned above, the model can also have interesting signatures at lepton flavour violating decays like $\mu \rightarrow e\gamma$, $\mu \rightarrow eee$ and $\mu \rightarrow e$ conversions [42, 43]. In this work, we examine one more way of probing this popular and predictive model indirectly. One such indirect possibility is to search for gravitational wave (GW) which has gained lots of attention due to planned near future experiments like LISA and other similar space based interferometer experiments [44–51].¹ A possible source of GW signals is a strong first-order phase transition (SFOPT) where, in particular, GW signals are generated by bubble collisions [54–58], the sound wave of the plasma [59–62] and the turbulence of the plasma [63–68]. The study of SFOPT is well-motivated in beyond the SM (BSM) with extended Higgs sectors, which allows for new source of CP violation and could produce baryon excess during the electroweak phase transition (EWPT). Therefore, it would be interesting to investigate if SFOPT can happen at high temperature in BSM. For a review of cosmological phase transitions and their experimental signatures, one may refer to the recent review article [69]. While a strong first-order EWPT is not possible in the SM alone due to high mass of SM like Higgs as confirmed by lattice studies [70, 71], addition of other scalars like the one in scotogenic model can allow the EWPT to be of first order. Several works have studied such interplay of DM and first order EWPT, specially in the presence of additional scalar doublet DM like we have in the present model [72–78]. While scalar doublet DM extension of the SM, popularly known as inert doublet model (IDM) allows a large parameter space supporting a SFOPT, most of this parameter space corresponds to sub-dominant DM [75] leaving a narrow window in low mass DM regime where both DM relic and SFOPT criteria can be simultaneously satisfied [73]. On the other hand, this low mass regime is getting increasingly in tension with direct search experiments as well as the collider constraints on invisible decay rate of the SM like Higgs, where the former remains much more stringent. In fact, we show that the parameter space of scalar DM which satisfies SFOPT is already disfavoured by Xenon1T data of 2018. Extending IDM to scotogenic model not only addresses the origin of light neutrino mass but also enlarges the parameter space that can simultaneously satisfy DM relic as well as SFOPT. We discuss the possibilities of both scalar and fermion DM in this model and constrain the parameter space from DM relic, SFOPT as well as light neutrino masses while

¹ These new sensitivity curves are presented in Refs. [52, 53].

incorporating relevant experimental and theoretical bounds. We then study the possibility of generating GW from such SFOPT and discuss the possibility of its detection in future experiments.²

This paper is organised as follows. In section II we discuss the model, particle spectrum and different constraints. In section III we review on the details of SFOPT and generation of GW. In section IV we briefly show how to calculate DM relic following thermal WIMP paradigm and then discuss our results in section V. We finally conclude in section VI.

II. MINIMAL SCOTOGENIC MODEL

The minimal scotogenic model is an extension of the SM by three copies of SM-singlet fermions N_i (with $i = 1, 2, 3$) and one $SU(2)_L$ -doublet scalar field S (called inert scalar doublet), all being odd under an in-built and unbroken Z_2 symmetry, while the SM fields remain Z_2 -even under the Z_2 -symmetry such that

$$N_i \rightarrow -N_i, \quad S \rightarrow -S, \quad \Phi \rightarrow \Phi, \quad \Psi_{\text{SM}} \rightarrow \Psi_{\text{SM}}, \quad (1)$$

where Φ is the SM Higgs doublet and Ψ_{SM} 's stand for the SM fermions. The unbroken Z_2 symmetry not only prevents the inert scalar doublet to acquire any non-zero vacuum expectation value (VEV) but also forbids Yukawa coupling of lepton doublets with Z_2 odd singlet fermions via SM Higgs, keeping neutrinos massless at tree level. The Yukawa interactions of the lepton sector can be written as

$$\mathcal{L} \supset \frac{1}{2}(M_N)_{ij}N_iN_j + \left(Y_{ij}\bar{L}_i\tilde{S}N_j + \text{h.c.}\right). \quad (2)$$

The tree level scalar potential of the model, V_{tree} , is given by

$$V_{\text{tree}} = \lambda_{\text{SM}} \left(\Phi^{\dagger i} \Phi_i - \frac{v_{\text{SM}}}{2} \right)^2 + m_1^2 S^{\dagger i} S_i + \lambda_1 (\Phi^{\dagger i} \Phi_i) (S^{\dagger j} S_j) + \lambda_2 (\Phi^{\dagger i} S_i) (S^{\dagger j} \Phi_j) + [\lambda_3 \Phi^{\dagger i} \Phi^{\dagger j} S_i S_j + \text{h.c.}] + \lambda_S (S^{\dagger j} S_j)^2. \quad (3)$$

Here, indices i and j represent $SU(2)$ isospin. The Z_2 symmetry prevents linear and trilinear terms of the inert doublet with the SM Higgs. The bare mass squared term of the inert scalar doublet is chosen to be positive definite in order to ensure that it does not acquire any

² See e.g. Ref. [79] for the detailed analysis of constraints coming from GW detections.

non-zero VEV. Absence of linear terms ensures that it does not even acquire any induced VEV after electroweak symmetry breaking (EWSB). The first term in Eq. (3) describes EWSB with $v_{\text{SM}} \simeq 246\text{GeV}$ and $\lambda_{\text{SM}} \simeq 0.13$. To compute mass spectrums of H and S fields, let us parametrise those fields as follows.

$$\Phi = \begin{pmatrix} 0 \\ \frac{\phi}{\sqrt{2}} \end{pmatrix}, \quad S = \begin{pmatrix} S^+ \\ S_0 \end{pmatrix}. \quad (4)$$

For S^+ and S_0 fields, we have following mass terms:

$$m_{\pm}^2 = m_1^2 + \frac{1}{2}\lambda_1\phi^2, \quad \mathcal{M}_{S_0}^2 = \begin{pmatrix} m_1^2 + \frac{1}{2}(\lambda_1 + \lambda_2 + 2\lambda_3)\phi^2, & 0 \\ 0, & m_1^2 + \frac{1}{2}(\lambda_1 + \lambda_2 - 2\lambda_3)\phi^2 \end{pmatrix}. \quad (5)$$

Using $S_0 = (H + iA)/\sqrt{2}$ we obtain the physical masses as

$$\begin{aligned} n_{\pm} = 2 & : m_{\pm}^2 = m_1^2 + \frac{1}{2}\lambda_1\phi^2, \\ n_H = 1 & : m_H^2 = m_1^2 + \frac{1}{2}(\lambda_1 + \lambda_2 + 2\lambda_3)\phi^2, \\ n_A = 1 & : m_A^2 = m_1^2 + \frac{1}{2}(\lambda_1 + \lambda_2 - 2\lambda_3)\phi^2, \end{aligned} \quad (6)$$

where m_H (m_A) and m_{\pm} are the masses of CP-even (odd) component and the charged component of the inert scalar doublet, respectively, and n_{\pm} , n_H and n_A represent degrees of freedom (dof) of each fields. Present masses are obtained by $\phi = v_{\text{SM}}$. In this notation, the SM Higgs mass is $m_h^2 = 2\lambda_{\text{SM}}\phi^2$.

While neutrinos remain massless at tree level, a non-zero mass can be generated at one-loop level given by [1, 80]

$$\begin{aligned} (M_{\nu})_{ij} &= \sum_k \frac{Y_{ik}Y_{jk}M_k}{32\pi^2} \left(\frac{m_H^2}{m_H^2 - M_k^2} \ln \frac{m_H^2}{M_k^2} - \frac{m_A^2}{m_A^2 - M_k^2} \ln \frac{m_A^2}{M_k^2} \right) \\ &\equiv \sum_k \frac{Y_{ik}Y_{jk}M_k}{32\pi^2} [L_k(m_H^2) - L_k(m_A^2)], \end{aligned} \quad (7)$$

where M_k is the mass eigenvalue of the mass eigenstate N_k in the internal line and the indices $i, j = 1, 2, 3$ run over the three neutrino generations as well as three copies of N_i .

The function $L_k(m^2)$ is defined as

$$L_k(m^2) = \frac{m^2}{m^2 - M_k^2} \ln \frac{m^2}{M_k^2}. \quad (8)$$

It is important to ensure that the choice of Yukawa couplings as well as other parameters involved in light neutrino mass are consistent with the cosmological upper bound on the sum of neutrino masses, $\sum_i m_i \leq 0.11$ eV [5], as well as the neutrino oscillation data [3, 4]. In order to incorporate these constraints on model parameters, it is often useful to rewrite the neutrino mass formula given in equation (7) in a form resembling the type-I seesaw formula:

$$M_\nu = Y\Lambda^{-1}Y^T, \quad (9)$$

where we have introduced the diagonal matrix Λ with elements

$$\Lambda_i = \frac{2\pi^2}{\lambda_3} \zeta_i \frac{M_i}{v^2}, \quad (10)$$

$$\text{and } \zeta_i = \left(\frac{M_i^2}{8(m_H^2 - m_A^2)} [L_i(m_H^2) - L_i(m_A^2)] \right)^{-1}. \quad (11)$$

The light neutrino mass matrix (9) which is complex symmetric, can be diagonalised by the usual Pontecorvo-Maki-Nakagawa-Sakata (PMNS) mixing matrix U ³, written in terms of neutrino oscillation data (up to the Majorana phases) as

$$U = \begin{pmatrix} c_{12}c_{13} & s_{12}c_{13} & s_{13}e^{-i\delta} \\ -s_{12}c_{23} - c_{12}s_{23}s_{13}e^{i\delta} & c_{12}c_{23} - s_{12}s_{23}s_{13}e^{i\delta} & s_{23}c_{13} \\ s_{12}s_{23} - c_{12}c_{23}s_{13}e^{i\delta} & -c_{12}s_{23} - s_{12}c_{23}s_{13}e^{i\delta} & c_{23}c_{13} \end{pmatrix} U_{\text{Maj}} \quad (12)$$

where $c_{ij} = \cos \theta_{ij}$, $s_{ij} = \sin \theta_{ij}$ and δ is the leptonic Dirac CP phase. The diagonal matrix $U_{\text{Maj}} = \text{diag}(1, e^{i\xi_1}, e^{i\xi_2})$ contains the undetermined Majorana CP phases ξ_1, ξ_2 . The diagonal light neutrino mass matrix is therefore,

$$D_\nu = U^\dagger M_\nu U^* = \text{diag}(m_1, m_2, m_3). \quad (13)$$

Since the inputs from neutrino data are only in terms of the mass squared differences and mixing angles, it would be useful for our purpose to express the Yukawa couplings in terms of light neutrino parameters. This is possible through the Casas-Ibarra (CI) parametrisation [81] extended to radiative seesaw model [42] which allows us to write the Yukawa coupling matrix satisfying the neutrino data as

$$Y = U D_\nu^{1/2} R^\dagger \Lambda^{1/2}, \quad (14)$$

where R is an arbitrary complex orthogonal matrix satisfying $RR^T = \mathbb{1}$.

³ Usually, the leptonic mixing matrix is given in terms of the charged lepton diagonalising matrix (U_l) and light neutrino diagonalising matrix U_ν as $U = U_l^\dagger U_\nu$. In the simple case where the charged lepton mass matrix is diagonal which is true in our model, we can have $U_l = \mathbb{1}$. Therefore we can write $U = U_\nu$.

A. Constraints on Model Parameters

Precision measurements at LEP experiment forbids additional decay channels of the SM gauge bosons. For example, it strongly constrains the decay channel $Z \rightarrow HA$ requiring $m_H + m_A > m_Z$. Additionally, LEP precision data also rule out the region $m_H < 80 \text{ GeV}, m_A < 100 \text{ GeV}, m_A - m_H > 8 \text{ GeV}$ [82]. We take the lower bound on charged scalar mass $m_{\pm} > 90 \text{ GeV}$. If $m_{H,A} < m_h/2$, the large hadron collider (LHC) bound on invisible Higgs decay comes into play [83] which can constrain the SM Higgs coupling with H, A namely $\lambda_1 + \lambda_2 \pm 2\lambda_3$ to as small as 10^{-4} , which however remains weaker than DM direct detection bounds in this mass regime (see for example, [84]).

The LHC experiment can also put bounds on the scalar masses in the model, though in a model dependent way. Depending upon the mass spectrum of its components, the heavier ones can decay into the lighter ones and a gauge boson, which finally decays into a pair of leptons or quarks. Therefore, we can have either pure leptonic final states plus missing transverse energy (MET), hadronic final states plus MET or a mixture of both. The MET corresponds to DM or light neutrinos. In several earlier works [14, 36, 37], the possibility of opposite sign dileptons plus MET was discussed. In [38], the possibility of dijet plus MET was investigated with the finding that inert scalar masses up to 400 GeV can be probed at high luminosity LHC. In another work [85], tri-lepton plus MET final states was also discussed whereas mono-jet signatures have been studied by the authors of [39, 40]. The enhancement in dilepton plus MET signal in the presence of additional vector like singlet charged leptons was also discussed in [86]. Exotic signatures like displaced vertex and disappearing or long-lived charged track for compressed mass spectrum of inert scalars and singlet fermion DM was studied recently by the authors of [41].

In addition to the collider or direct search constraints, there exists theoretical constraints also. For instance, the scalar potential of the model should be bounded from below in any field direction. This criteria leads to the following co-positivity conditions. [15, 87–89]:

$$\lambda_S > 0, \lambda_1 + 2\sqrt{\lambda_{\text{SM}}\lambda_S} > 0, \lambda_1 + \lambda_2 - \frac{|\lambda_3|}{2} + 2\sqrt{\lambda_{\text{SM}}\lambda_S} > 0. \quad (15)$$

The last condition comes from unitarity of the S -matrix elements [90, 91]. The coupling constants appeared in above expressions are evaluated at the electroweak scale, v_{SM} . Also, in order to avoid perturbative breakdown, all dimensionless couplings like quartic couplings

(λ_i), Yukawa couplings (Y_{ij}), gauge couplings (g_i) should obey the the perturbativity conditions:

$$|\lambda_i| < 4\pi, |Y_{ij}| < \sqrt{4\pi}, g_i < \sqrt{4\pi} \quad (16)$$

where indices run over appropriate numbers according to the Lagrangian.

III. SFOPT AND PRODUCTION OF GW

The main purpose of this section is to show how to calculate the finite-temperature effective potential and GW signals generated by a first-order phase transition. The crucial difference from the previous analysis done in Ref. [73] is that we here include effects of resummation in order to account for IR divergences in finite-temperature field theory, and explicitly calculate GW signals.

A. Finite-temperature effective potential

In this subsection, we calculate the one-loop effective potential at finite-temperature. A total effective potential can be schematically divided into following form:

$$V_{\text{tot}} = V_{\text{tree}} + V_{\text{CW}} + V_{\text{th}}, \quad (17)$$

where V_{tree} , V_{CW} and V_{th} denote the tree level scalar potential, the one-loop Coleman-Weinberg potential, the thermal effective potential, respectively. The tree level scalar potential is given by Eq. (3). In finite-temperature field theory, the effective potential, V_{CW} and V_{thermal} , are calculated by using standard background field method [92, 93]. In the following calculations, we take Landau gauge for simplicity.⁴

The Coleman-Weinberg potential [96] with $\overline{\text{DR}}$ regularisation is given by

$$V_{\text{CW}} = \sum_i (-)^{n_f} \frac{n_i}{64\pi^2} m_i^4(\phi) \left(\log \left(\frac{m_i^2(\phi)}{\mu^2} \right) - \frac{3}{2} \right), \quad (18)$$

where suffix i represents particle species, and n_i , $m_i(\phi)$ are the degrees of freedom (d.o.f) and field dependent masses of i 'th particle. In addition, μ is the renormalisation scale, and

⁴ The gauge dependence of the thermal effective potential is discussed by many authors. See. e.g. Refs. [94, 95] and references therein.

$(-)^{n_f}$ is +1 for bosons and -1 for fermions, respectively. In our analysis, for simplicity, we take the renormalisation scale as $\mu = v_{\text{SM}}$ because the electroweak scale is the only relevant energy scale. We confirm that nucleation temperatures are around at electroweak scale for the whole region of the parameter space, and thus, the one-loop calculation is validated with this choice. (For the definition of the nucleation temperature, see Eq. (38) in the next subsection.)

Thermal contributions to the effective potential are given by

$$V_{\text{th}} = \sum_i \left(\frac{n_{B_i}}{2\pi^2} T^4 J_B \left[\frac{m_{B_i}}{T} \right] - \frac{n_{F_i}}{2\pi^2} J_F \left[\frac{m_{F_i}}{T} \right] \right), \quad (19)$$

where n_{B_i} and n_{F_i} denote the dof of the bosonic and fermionic particles, respectively. In this expressions, J_B and J_F functions are defined by following functions:

$$J_B(x) = \int_0^\infty dz z^2 \log \left[1 - e^{-\sqrt{z^2+x^2}} \right], \quad (20)$$

$$J_F(x) = \int_0^\infty dz z^2 \log \left[1 + e^{-\sqrt{z^2+x^2}} \right]. \quad (21)$$

In our analysis, we do not use high-temperature expansions only validated for small x to evaluate $J_B(x)$ and $J_F(x)$. One should note that a potential barrier arises from $J_B(x)$ which triggers a first-order phase transition. Therefore, the strong first-order electroweak phase transition requires bosons strongly coupled to the Higgs field. (See next subsection for the definition of the SFOPT.) In comparison to the SM, this model contains an additional $SU(2)_W$ inert scalar doublet, and thus, the strong first-order electroweak phase transition takes place as we will see Sec. V.

For a calculation of V_{th} , we include a contribution from daisy diagram to improve the perturbative expansion during the phase transition [97–99]. The daisy improved effective potential can be calculated by inserting thermal masses into the zero-temperature field dependent masses. The author of Ref. [98] proposed the thermal resummation prescription in which the thermal corrected field dependent masses are used for the calculation in V_{CW} and V_{th} (Parwani method). In comparison to this prescription, authors of Ref. [99] proposed alternative prescription for the thermal resummation (Arnold-Espinosa method). They include the effect of daisy diagram only for Matsubara zero-modes inside J_B function defined in Eq. (20). A qualitative difference between two prescriptions is discussed in Ref. [100]. For simplicity, we here use former (Parwani method) prescription in order to implement daisy resummation in the public code `CosmoTransitions` [101].

The thermal mass for the inert scalar doublet, $\Pi_S(T)$, is calculated in Ref. [76] as

$$\Pi_S = \left(\frac{1}{8}g_2^2 + \frac{1}{16}(g_1^2 + g_2^2) + \frac{1}{2}\lambda_S + \frac{1}{12}\lambda_1 + \frac{1}{24}\lambda_A + \frac{1}{24}\lambda_H \right) T^2. \quad (22)$$

where $\lambda_A = \lambda_1 + \lambda_2 - 2\lambda_3$ and $\lambda_H = \lambda_1 + \lambda_2 + 2\lambda_3$, and g_1 and g_2 are the gauge coupling of $SU(2)_W$ and $U(1)_Y$, respectively. One should note that the Yukawa coupling between the inert doublet and the neutrino given by Eq. (2) may give an additional contribution to $\Pi_S(T)$. However, since the right-handed neutrino has Majorana mass comparable to the nucleation temperature, this effect would be suppressed due to the Boltzmann suppression in finite-temperature, and hence, we expect that this contribution will not change our result significantly. We therefore neglect this contribution in our analysis.

For gauge bosons, the longitudinal mode and the transverse mode obtain different thermal masses called Debye mass and the magnetic mass, respectively [102]. Since the magnetic mass is subdominant, we only calculate the Debye mass for $SU(2)_W \times U(1)_Y$ gauge bosons. The Debye mass can be estimated by using SM result [103, 104] with adding an additional $SU(2)_W$ inert scalar doublet as

$$\Pi_W = 2g_2^2T^2, \quad \Pi_Y = 2g_1^2T^2. \quad (23)$$

The field dependent masses are obtained by diagonalising mass matrices for $SU(2)_W \times U(1)_Y$ gauge bosons and neutral component of the inert scalar doublet.

We consider contributions coming from inert scalar doublet, $SU(2)_W \times U(1)_Y$ gauge bosons and top quarks because those couplings are large compared to other particles. Field

dependent masses and d.o.f are then listed as

$$n_{\pm} = 2 : m_{\pm}^2(\phi) = m_1^2 + \frac{\lambda_1}{2}\phi^2 + \Pi_S(T), \quad (24)$$

$$n_H = 1 : m_H^2(\phi) = m_1^2 + \frac{1}{2}\lambda_H\phi^2 + \Pi_S(T), \quad (25)$$

$$n_A = 1 : m_A^2(\phi) = m_1^2 + \frac{1}{2}\lambda_A\phi^2 + \Pi_S(T), \quad (26)$$

$$n_W = 4 : m_W^2(\phi) = \frac{g_2^2}{4}\phi^2, \quad (27)$$

$$n_Z = 2 : m_Z^2(\phi) = \frac{(g_1^2 + g_2^2)}{4}\phi^2, \quad (28)$$

$$n_{W_L} = 2 : m_{W_L}^2(\phi) = \frac{g_2^2}{4}\phi^2 + \Pi_W(T), \quad (29)$$

$$n_{Z_L} = 1 : m_{Z_L}^2(\phi) = \frac{1}{2}(m_Z^2(\phi) + \Pi_W(T) + \Pi_Y(T) + \Delta(\phi, T)), \quad (30)$$

$$n_{\gamma_L} = 1 : m_{\gamma_L}^2(\phi) = \frac{1}{2}(m_Z^2(\phi) + \Pi_W(T) + \Pi_Y(T) - \Delta(\phi, T)), \quad (31)$$

$$\Delta^2(\phi, T) \equiv \left(\frac{g_2^2}{4}\phi^2 + \Pi_W(T) - \frac{g_1^2}{4}\phi^2 - \Pi_Y(T) \right)^2 + 4g_1^2g_2^2\phi^4. \quad (32)$$

The last contribution comes from the longitudinal mode of the massive photon.

B. First-order phase transitions and GW signals

In this subsection, we briefly review basics of the first-order phase transition and GW production. When the phase transition proceeds via the tunnelling, we call it the first-order phase transition. If the phase transition is of first order, the spherical symmetric field configurations called bubbles are nucleated in the early universe. Then they expand and eventually coalesce with each other.

The tunnelling rate per unit time and per unit volume, Γ , is given by

$$\Gamma(T) = \mathcal{A}(T)e^{-\mathcal{B}}, \quad (33)$$

where $\mathcal{A}(T) \sim T^4$ and \mathcal{B} are determined by the dimensional analysis and given by the classical configurations, called bounce, respectively. At finite-temperature, the $O(3)$ symmetric bounce solution is favoured [105] for the case without significant supercooling. The $O(3)$ symmetric bounce solution is calculated by solving the differential equation given by

$$\frac{d^2\phi}{dr^2} + \frac{2}{r}\frac{d\phi}{dr} = \frac{\partial V_{\text{tot}}}{\partial\phi}, \quad (34)$$

with the following boundary conditions:

$$\phi(r \rightarrow \infty) = \phi_{\text{false}}, \quad \left. \frac{d\phi}{dr} \right|_{r=0} = 0. \quad (35)$$

In this expression, ϕ_{false} denotes the position of the false vacuum. Then the $O(3)$ symmetric bounce action is given by

$$S_3 = \int_0^\infty dr 4\pi r^2 \left[\frac{1}{2} \left(\frac{d\phi}{dr} \right)^2 + V_{\text{tot}}(\phi, T) \right], \quad (36)$$

where ϕ satisfies equation of motion given by Eqs. (34) and (35).

The nucleation temperature defined as the temperature when bubbles are nucleated, T_n , is conservatively estimated by comparing the tunnelling rate to the Hubble parameter as

$$\Gamma(T_n) = \mathbf{H}^4(T_n). \quad (37)$$

Here, the Hubble parameter is given by $\mathbf{H}(T) \simeq 1.66\sqrt{g_*}T^2/M_{\text{Pl}}$ with g_* being the dof of the radiation component. Then above condition turns out to be

$$\frac{S_3(T_n)}{T_n} \simeq 140, \quad (38)$$

for $g_* \sim 100$ and $T_n \sim 100$ GeV. We evaluate bounce action by using public code `cosmoTransitions` [101] written in Python. If $\phi(T_n)/T_n > 1$ is satisfied, where $\phi(T_n)$ is the Higgs VEV at the nucleation temperature, $T = T_n$, the electroweak phase transition is called "strong" first order.

Amplitudes and frequencies of the GW are mainly determined by two parameters. One is the ratio of the amount of vacuum energy released by the phase transition to the radiation energy density of the universe, $\rho_{\text{rad}} = g_*\pi^2 T^4/30$, given by

$$\alpha = \frac{\epsilon}{\rho_{\text{rad}}}, \quad (39)$$

with

$$\epsilon = \Delta V_{\text{tot}} - \frac{T}{4} \frac{\partial \Delta V_{\text{tot}}}{\partial T}, \quad (40)$$

where $\Delta V_{\text{tot}} \equiv V_{\text{tot}}(\phi_{\text{false}}) - V_{\text{tot}}(\phi_{\text{true}})$ is the free energy difference between the false and true vacuum. ϵ is related to the change in the trace of the energy-momentum tensor across the bubble wall (See e.g. Refs. [49, 106] for detailed studies).

The another important parameter is duration of the phase transition denoted by β which is the characteristic time scale of the phase transition. β is defined as the time variation of the tunnelling rate of the phase transition given by [48]

$$\frac{\beta}{\mathbf{H}(T)} \simeq T \frac{d}{dT} \left(\frac{S_3}{T} \right). \quad (41)$$

Both parameters α and β are evaluated at $T = T_n$.

Let us next review the basic of GW signals generated by first-order phase transitions. There are three sources producing GWs : bubble collisions, sound wave of the plasma, and turbulence of the plasma. As confirmed in Refs. [107, 108], a contribution from bubble collisions is always subdominant for the case with small supercooling, $\alpha < 1$, since the bubble kinetic energy is almost converted into the thermal plasma due to the process called "transition radiation". We therefore consider contributions coming from thermal plasma, especially, the sound wave and the turbulence. Thus, total contribution to the GW signals can be decomposed into the following form:

$$\Omega_{\text{tot}} h^2 \simeq \Omega_{\text{sound}} h^2 + \Omega_{\text{tur}} h^2, \quad (42)$$

where Ω_{sound} and Ω_{tur} are the contributions from the sound wave and the turbulence of the plasma, respectively.

The contribution coming from sound wave of the plasma is estimated in Refs. [48, 61, 67, 109] as

$$\Omega_{\text{sound}} h^2 = 2.65 \times 10^{-6} \times \mathbf{H} \tau_{\text{sound}} \left(\frac{\mathbf{H}(T_n)}{\beta} \right) \left(\frac{\kappa_{\text{sound}} \alpha}{1 + \alpha} \right)^2 \left(\frac{100}{g_*} \right)^{\frac{1}{3}} v_w \left(\frac{f}{f_{\text{sound}}} \right)^3 \left[\frac{7}{4 + 3 \left(\frac{f}{f_{\text{sound}}} \right)^2} \right]^{\frac{7}{2}}, \quad (43)$$

where κ_{sound} and v_w are the efficiency factor and the bubble wall velocity, respectively. The factor $\mathbf{H} \tau_{\text{sound}}$ represents a suppression factor coming from the short-lasting sound wave as originally pointed out in Ref. [110] (Also, See e.g. Refs. [111, 112].) and is given by

$$\mathbf{H} \tau_{\text{sound}} = \min \left\{ 1, (8\pi)^{\frac{1}{3}} \left(\frac{\max\{c_s, v_w\}}{\beta/\mathbf{H}(T_n)} \right) \left(\frac{4}{3} \frac{1 + \alpha}{\kappa_{\text{sound}} \alpha} \right)^{\frac{1}{2}} \right\}. \quad (44)$$

Here c_s is the speed of sound wave in the plasma and f_{sound} is the peak frequency of the GW signals given by

$$f_{\text{sound}} = 1.9 \times 10^{-2} \text{mHz} \times \frac{1}{v_w} \left(\frac{\beta}{\mathbf{H}(T_n)} \right) \left(\frac{T_n}{100 \text{GeV}} \right) \left(\frac{g_*}{100} \right)^{\frac{1}{6}}. \quad (45)$$

We here simply estimate the bubble wall velocity by adopting following formula [113]⁵:

$$v_w = \frac{1/\sqrt{3} + \sqrt{\alpha^2 + 2\alpha/3}}{1 + \alpha}. \quad (46)$$

With above bubble wall velocity called Jouguet detonations, the efficiency factor, κ_{sound} , is fitted by following formula as found in Ref. [118]:

$$\kappa_{\text{sound}} = \frac{\sqrt{\alpha}}{0.135 + \sqrt{0.98 + \alpha}}. \quad (47)$$

The contribution from turbulence plasma is estimated in Refs. [67, 109] as

$$\Omega_{\text{tur}} h^2 = 3.35 \times 10^{-4} \left(\frac{\mathbf{H}(T_n)}{\beta} \right) \left(\frac{\kappa_{\text{tur}} \alpha}{1 + \alpha} \right)^{\frac{3}{2}} \left(\frac{100}{g_*} \right)^{\frac{1}{3}} v_w \frac{\left(\frac{f}{f_{\text{tur}}} \right)^3}{\left(1 + \left(\frac{f}{f_{\text{tur}}} \right) \right)^{\frac{11}{3}} \left(1 + \frac{8\pi f}{H_0} \right)}, \quad (48)$$

where κ_{tur} is the efficiency factor of the turbulence. κ_{tur} , H_0 and the peak frequency, f_{tur} , are given by

$$\kappa_{\text{tur}} \simeq 0.1 \kappa_{\text{sound}}, \quad (49)$$

$$H_0 \simeq 1.65 \times 10^{-4} \text{mHz} \times \left(\frac{T_n}{100 \text{GeV}} \right) \left(\frac{g_*}{100} \right)^{\frac{1}{6}}, \quad (50)$$

$$f_{\text{tur}} = 2.7 \times 10^{-2} \text{mHz} \left(\frac{1}{v_w} \right) \left(\frac{T_n}{100 \text{GeV}} \right) \left(\frac{\beta}{\mathbf{H}(T_n)} \right) \left(\frac{g_*}{100} \right)^{\frac{1}{6}}. \quad (51)$$

IV. DARK MATTER

The lightest Z_2 odd particle, if electromagnetically neutral, is the DM candidate in the model. Among the two scalar DM candidates H, A , we consider H as the DM, without any loss of generality. In the fermion DM scenario, the lightest right handed neutrino N_1 is the DM candidate. The relic abundance calculation of DM follows the usual approach of Boltzmann equation. If DM is of WIMP type and hence was produced thermally in the early universe, the evolution of its number density n_{DM} can be tracked by solving the Boltzmann equation

$$\frac{dn_{\text{DM}}}{dt} + 3\mathbf{H}n_{\text{DM}} = -\langle\sigma v\rangle [n_{\text{DM}}^2 - (n_{\text{DM}}^{\text{eq}})^2], \quad (52)$$

⁵ See Refs. [114–117], however, for the discussion of the bubble wall velocity v_w .

where $n_{\text{DM}}^{\text{eq}}$ is the equilibrium number density of DM and $\langle\sigma v\rangle$ is the thermally averaged annihilation cross section, given by [119]

$$\langle\sigma v\rangle = \frac{1}{8m_{\text{DM}}^4 T K_2^2\left(\frac{m_{\text{DM}}}{T}\right)} \int_{4m_{\text{DM}}^2}^{\infty} \sigma(s - 4m_{\text{DM}}^2) \sqrt{s} K_1\left(\frac{\sqrt{s}}{T}\right) ds, \quad (53)$$

where $K_i(x)$'s are modified Bessel functions of order i . In the presence of coannihilations, the effective cross section at freeze-out can be expressed as [120]

$$\sigma_{\text{eff}} = \sum_{i,j}^N \langle\sigma_{ij}v\rangle \frac{g_i g_j}{g_{\text{eff}}^2} (1 + \Delta_i)^{3/2} (1 + \Delta_j)^{3/2} e^{-z_f(\Delta_i + \Delta_j)}, \quad (54)$$

where $\Delta_i = \frac{m_i - m_{\text{DM}}}{m_{\text{DM}}}$ is the relative mass difference between the heavier component i of the inert Higgs doublet (with g_i internal dof) and the DM,

$$g_{\text{eff}} = \sum_{i=1}^N g_i (1 + \Delta_i)^{3/2} e^{-z_f \Delta_i} \quad (55)$$

is the total effective dof, and

$$\begin{aligned} \langle\sigma_{ij}v\rangle &= \frac{z_f}{8m_i^2 m_j^2 m_{\text{DM}} K_2\left(\frac{m_i z_f}{m_{\text{DM}}}\right) K_2\left(\frac{m_j z_f}{m_{\text{DM}}}\right)} \\ &\times \int_{(m_i + m_j)^2}^{\infty} ds \sigma_{ij}(s - 2(m_i^2 + m_j^2)) \sqrt{s} K_1\left(\frac{\sqrt{s} z_f}{m_{\text{DM}}}\right) \end{aligned} \quad (56)$$

is the modified thermally averaged cross section, compared to equation (53). In the above expressions

$$z_f \equiv \frac{m_{\text{DM}}}{T_f} = \ln\left(0.038 \frac{g}{\sqrt{g_*}} M_{\text{Pl}} m_{\text{DM}} \langle\sigma v\rangle_f\right), \quad (57)$$

with g being the number of internal DOF of the DM and the subscript f on $\langle\sigma v\rangle$ means that the quantity is evaluated at the freeze-out temperature T_f . The freeze-out temperature corresponds to the epoch where the rate of interaction equals that of the expansion, $\Gamma(T = T_f) = \mathbf{H}(T = T_f)$. Since N_1 is a gauge singlet, there exists the possibility of non-thermal fermion DM also in this model, as discussed by [22]. While the scalar DM can not be a purely non-thermal DM due to its gauge interactions, it can receive a non-thermal contribution from right handed neutrino decay at late epochs, as discussed by [19]. We do not discuss such possibilities in this work, as it is unlikely to give new insights into the correlation between DM parameter space and that of SFOPT. For solving the Boltzmann equations relevant to DM, we have used `micrOMEGAs` package [121].

V. RESULTS AND DISCUSSION

In this section, we discuss our results obtained after performing a full numerical scan by incorporating all existing constraints and the criteria for a SFOPT and the correct DM relic density. In this parameter search, we vary the parameters m_1 , λ_1 , λ_2 , λ_3 and λ_S . While all four parameters are relevant for SFOPT, the last one does not affect the DM relic abundance. We have also imposed the LEP bounds as well as the perturbative and vacuum stability conditions discussed earlier. The constraints coming from light neutrino masses are incorporated by using Casas-Ibarra parametrisation discussed before.

We here qualitatively comment on the strength of the electroweak phase transition. As we already noted in Sec. III A, the strong first-order electroweak phase transition is realised when additional bosons present in the model strongly couple to the SM Higgs. In this model, the inert scalar doublet, S , couples to the SM Higgs, and thus, larger λ_H , λ_A and λ_1 make the phase transition strength stronger. Also, larger m_1 makes the phase transition strength weaker due to the screening effect [93]. For the same reason, since a larger λ_S corresponds to larger thermal mass of the inert scalar (See Eq. (22)), it makes the phase transition strength weaker. Therefore the strong first-order electroweak phase transition requires larger λ_H , λ_A and λ_1 , and smaller m_1 and λ_S . Quantitative discussions are presented in each subsections below which are created according to the choice of DM candidate in the minimal scotogenic model.

A. Scalar dark matter

In this subsection, we show some results in the case of scalar DM scenario. In addition to collider bounds, the perturbative and the vacuum stability conditions, we impose conditions $\lambda_3 < 0$ and $\lambda_2 + 2\lambda_3 < 0$ in order to make CP even component of inert doublet H to be DM candidate.

We show the data points satisfying the conditions $\phi(T_n)/T_n > 1$ on (m_{\pm}, m_A) -plane in upper panel of Fig. 1. While DM mass can be low $m_H < 80$ GeV, the charged and neutral pseudo scalar masses are required to be large. In lower left panel of Fig. 1 we show the parameter region on (m_{\pm}, m_A) -plane which satisfies $\Omega_{\text{DM}}h^2 = 0.120 \pm 0.001$ with varying DM mass shown as colour code. This clearly shows the two distinct regions of

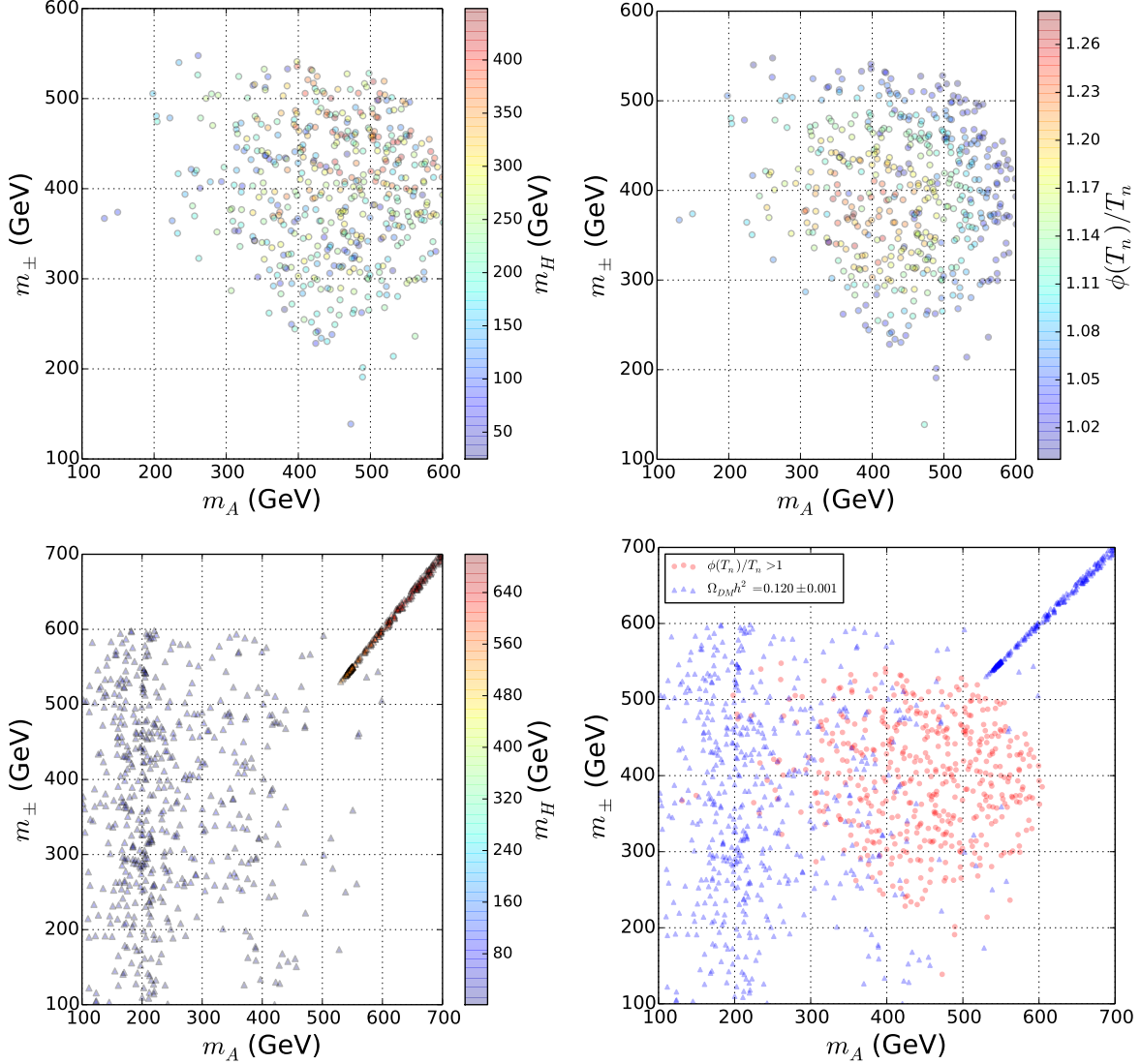


FIG. 1. Scatter plots on (m_{\pm}, m_A) -plane satisfying $\phi(T_n)/T_n > 1$ for different scalar DM mass, m_H , (upper left) and the strength of the electroweak phase transition $\phi(T_n)/T_n$ (upper right) are shown in the case of scalar DM scenario. A parameter regime satisfying $\Omega_{\text{DM}}h^2 = 0.120 \pm 0.001$ for different DM mass (lower left) and a combined scatter plot (lower right) for $\phi(T_n)/T_n > 1$ (red circles) and $\Omega_{\text{DM}}h^2 = 0.120 \pm 0.001$ (blue triangles) are also shown.

DM (H) mass: $m_H < 80$ GeV and $m_H > 550$ GeV typical of inert doublet dark matter known in the literature. In the lower right panel we also superimpose the points which satisfy the SFOPT criteria, showing overlap with parameter space corresponding to low mass DM. We confirm that there is a parameter regime satisfying conditions $\phi(T_n)/T_n > 1$ and $\Omega_{\text{DM}}h^2 = 0.120 \pm 0.001$, specially for low DM mass $m_H < 80$ GeV. One should note that

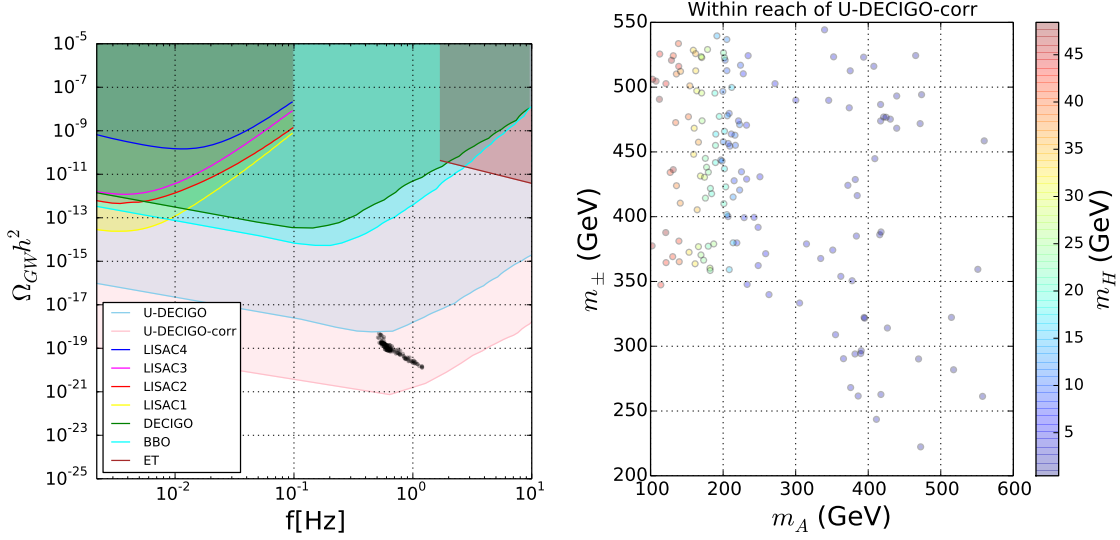


FIG. 2. Left panel: peak points of GW signals in our model along with sensitivity curves of U-DECIGO, U-DECIGO-corr, LISAC1~C4 [48, 122], DECIGO, BBO [123] and Einstein Telescope (ET) [124, 125]. Scatter plots on (m_{\pm}, m_A) -plane within reach of U-DECIGO with a correlation analysis (U-DECIGO-corr) [50] for different m_H (right panel) are shown in the case of scalar DM. All data points satisfy correct DM relic density, $\Omega_{\text{DM}}h^2 = 0.120 \pm 0.001$.

the SF OPT requires fine-tuning between λ_1 and $\lambda_2 + 2\lambda_3$ to maintain small $\lambda_H = \lambda_1 + \lambda_2 + 2\lambda_3$ for a low DM mass regime, $m_H < 80\text{GeV}$, as originally pointed out by authors of Ref. [73]. While the DM relic satisfying points in low mass regime remain scattered, there is a linear correlation in high mass regime beyond 550 GeV, as can be seen from bottom panel plots of Fig. 1. This arises because of the fact that, in order to satisfy correct DM relic in high mass regime $m_H > 550\text{GeV}$, the mass splitting between inert doublet components is required to be small. We also find that SF OPT criteria requires the bare mass parameter of inert doublet to be small $0 < m_1/\text{GeV} < 50$. Therefore, in the large DM mass regime, $m_H > 550\text{GeV}$, we need larger values of m_1 making the phase transition strength weaker, and thus, it is difficult to realise $\phi(T_n)/T_n > 1$ with imposing perturbative conditions $|\lambda_i| < 4\pi$ ($i = 1, 2, 3$). Thus, the low mass DM region $m_H < 80\text{GeV}$ is the preferred region from SF OPT and DM relic point of view in the scalar DM scenario of this model.

In left panel of Fig. 2, we show total GW signals with sensitivity curves of several future planned space based experiments like U-DECIGO, U-DECIGO-corr, LISA (C1-C4) [48, 122], DECIGO, BBO [123] and Einstein Telescope (ET) [124, 125] along with the black dotted

region corresponding to our model in scalar DM scenario. Clearly, the strength of the GW signal in our model is within the reach of only U-DECIGO-corr, a future space-based GW antenna [50, 51]. The corresponding region of model parameter space is shown in (m_{\pm}, m_A) -plane by taking points within the sensitivity of U-DECIGO-corr (right panel of Fig. 2). In this figure, the DM relic criteria $\Omega_{\text{DM}}h^2 = 0.120 \pm 0.001$ is imposed for all the points. We find that the total fraction of points in the parameter scan within the reach of U-DECIGO-corr is 39%. However, in this parameter regime, there is a fine-tuning between λ_1 and $\lambda_2 + 2\lambda_3$ in order to keep the scalar DM in low mass regime, as noted earlier. We do not investigate such fine-tuned region further in our study. Therefore, in the case of the scalar DM scenario, we conclude that it is difficult to produce detectable GW signals by U-DECIGO-corr while simultaneously giving rise to observed scalar DM relic without fine-tuning. As noted earlier, this low mass DM region is also tightly constrained by direct search and collider experiments. We in fact projected these data points to the direct detection cross section versus DM mass plane and find that they are already disfavoured by Xenon1T data, as seen from figure 3. While low mass DM is not completely ruled out yet by Xenon1T, the region satisfying SFOPT criteria is ruled out. As can be seen from the green coloured points in this figure, the region around the Higgs resonance $m_{\text{DM}} = m_H = m_h/2$ is still allowed. However these green coloured points do not give rise to the required SFOPT. This happens due to the requirement of small $m_1 \in (0, 50)\text{GeV}$ for SFOPT which further requires larger λ_H to keep DM mass near the Higgs resonance area. However, same λ_H also leads to spin-independent DM-nucleon scattering giving rise to tension with Xenon1T bounds. As we will see in the next subsection, the fine-tuning associated with scalar DM will be alleviated and stringent direct detection constraints will disappear in the case of the fermion DM scenario.

B. Fermion dark matter

In this subsection, we show the results in the case of the fermion DM scenario. Here we do not impose conditions $\lambda_3 < 0$ and $\lambda_2 + 2\lambda_3 < 0$ because as long as lightest singlet fermion N_1 is the lightest Z_2 odd particle, there is no restriction on the mass ordering among components of inert scalar doublet.

We show the parameter regime satisfying the conditions $\phi(T_n)/T_n > 1$ in (m_{\pm}, m_A) -plane in upper panel of Fig. 4 in the case of the fermion DM scenario. As one can see from

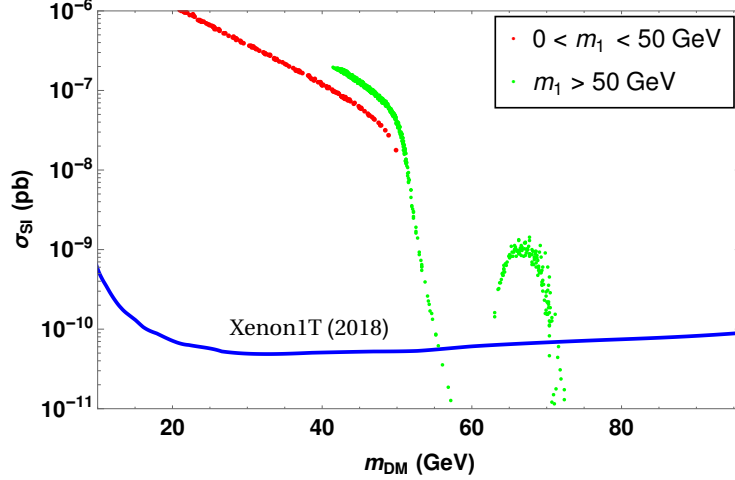


FIG. 3. Spin independent DM-nucleon cross section for scalar DM. The red coloured points satisfy the SFOPT criteria.

upper panels of Fig. 4, we additionally have a parameter regime satisfying $\phi(T_n)/T_n > 1$ for small values of m_{\pm} and m_A compared to what we found in the scalar DM scenario. This fact can be understood as following way. Since $\phi(T_n)/T_n > 1$ can be realised for smaller λ_1 (corresponding to smaller m_{\pm}) by making λ_H larger (corresponding to larger m_H) with fixed m_1 , a lower m_{\pm} region can lead to $\phi(T_n)/T_n > 1$ in comparison to the scalar DM scenario. This is a crucial difference from similar SFOPT analysis in IDM where the mass ordering within inert doublet components is always restricted to having one of the neutral components as the lightest. While sub-dominant scalar DM leads to more allowed region satisfying SFOPT as shown by [75], relaxing the mass ordering leads to even newer allowed region of parameter space. This has been made possible in scotogenic model where fermion DM remains a viable possibility. While in the upper panel plots of Fig. 4, the DM relic constraint is not implemented, we do so in the lower panel plots of the same figure. The lower left panel shows the parameter space in (m_{\pm}, m_A) -plane which satisfied the correct fermion DM relic while showing the fermion DM mass in colour code. The right lower panel plot shows the points satisfying SFOPT and DM relic criteria on (m_{\pm}, m_A) -plane clearly depicting overlap where both are satisfied. The points satisfying the fermion DM relic correspond to small λ_3 so that the Yukawa couplings (in $Y_{i1} \bar{L}_i \tilde{S} N_1$) are sizeable enough to enhance fermion DM annihilation and coannihilation channels. This correspondence between small λ_3 and large Yukawa arises through Casas-Ibarra parametrisation discussed

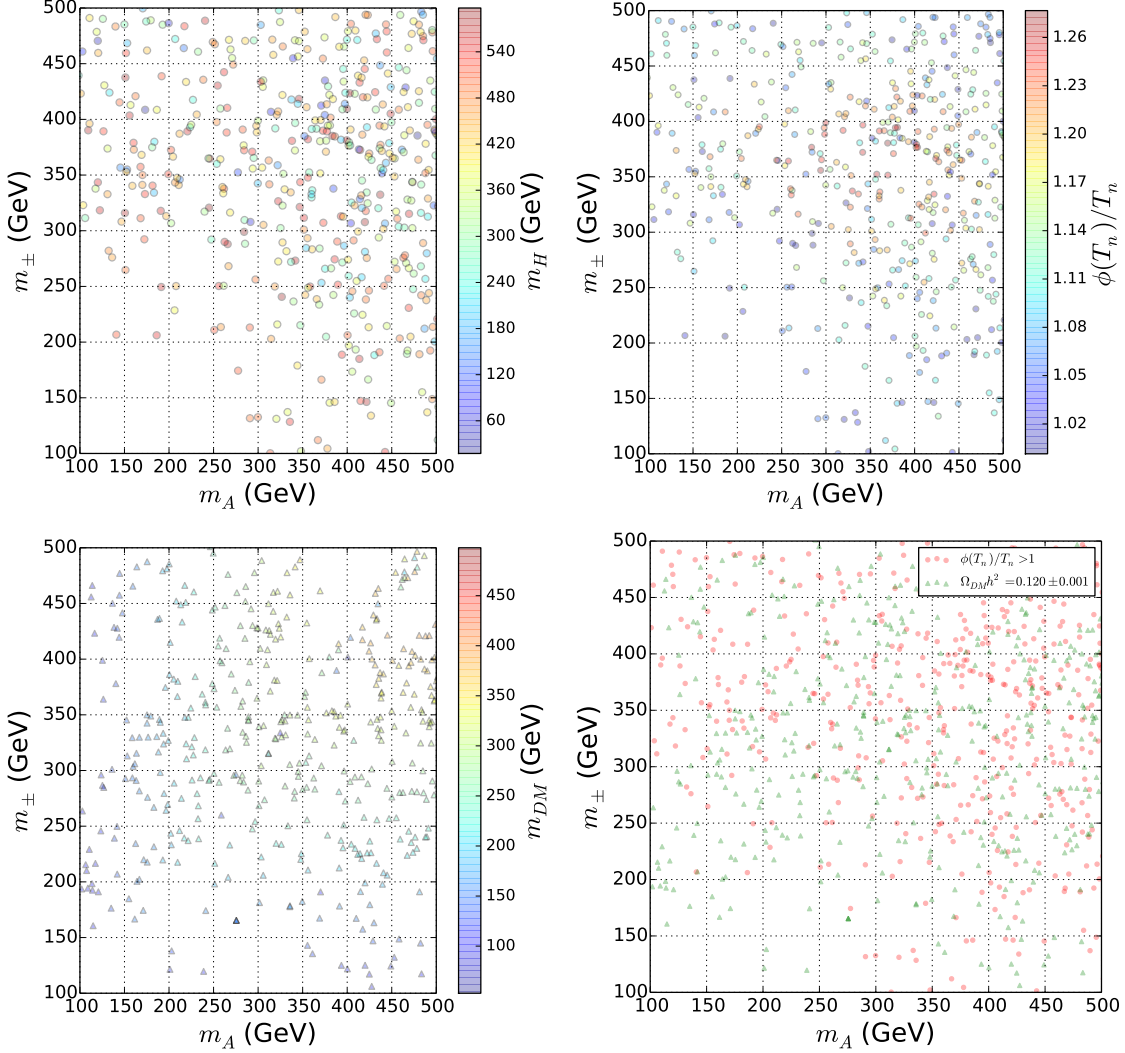


FIG. 4. Scatter plots on (m_{\pm}, m_A) -plane satisfying $\phi(T_n)/T_n > 1$ for different m_H , (upper left) and the strength of the electroweak phase transition $\phi(T_n)/T_n$ (upper right) are shown in the case of fermion DM scenario. A parameter regime satisfying $\Omega_{\text{DM}}h^2 = 0.120 \pm 0.001$ for different m_H (lower left) and a combined scatter plot (lower right) for $\phi(T_n)/T_n > 1$ (red circles) and $\Omega_{\text{DM}}h^2 = 0.120 \pm 0.001$ (green triangles) are also shown.

earlier. We consider lightest neutrino mass 0.1 eV in order to enhance the Yukawa couplings. Small λ_3 gives rise to almost degenerate H, A in this scenario.

We also show peak amplitudes of total GW signals in our model with fermion DM scenario along with sensitivity curves of different planned future experiments in left panel of Fig. 5. We then show scatter plots in (m_{\pm}, m_A) -plane by taking points within reach of U-DECIGO-corr and satisfying $\Omega_{\text{DM}}h^2 = 0.120 \pm 0.001$ in right panel of Fig. 5, respectively. Since there

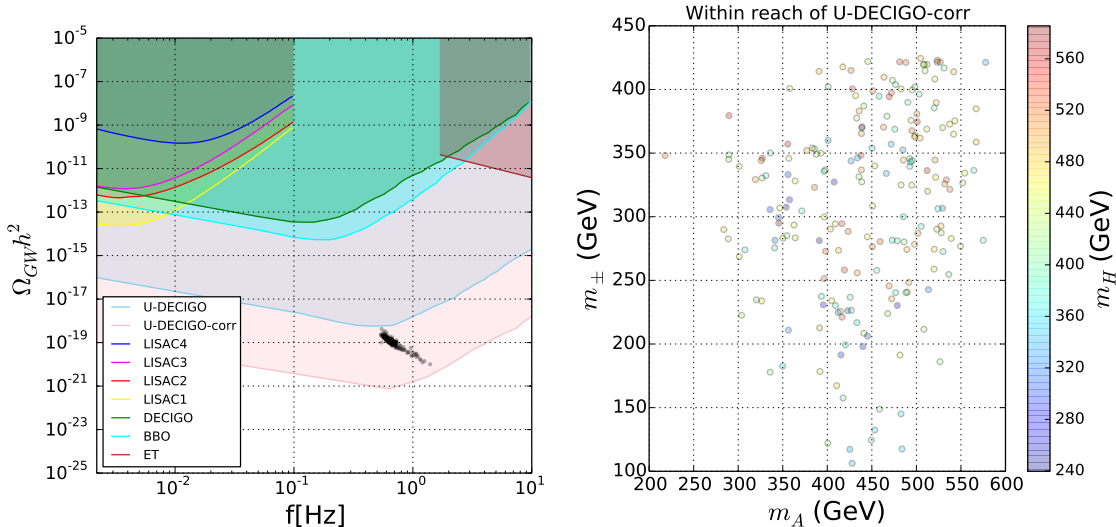


FIG. 5. Left panel: peak points of GW signals along with sensitivity curves of U-DECIGO, U-DECIGO-corr, LISAC1~C4, DECIGO, BBO and ET. Scatter plots on (m_{\pm}, m_A) -plane within reach of U-DECIGO-corr for different m_H (right panel) is shown in the case of fermion DM scenario. All data points satisfy correct DM relic density, $\Omega_{\text{DM}} h^2 = 0.120 \pm 0.001$.

is no restriction on the scalar mass ordering within inert scalar doublet in the case of the fermion DM scenario, GW signals can be easily enhanced by making λ_H large compared to the scalar DM scenario. Indeed, we find that the total fraction of points in the parameter scan within the reach of U-DECIGO-corr is 58%, which is larger than the one in the case of scalar DM scenario. Unlike in scalar DM scenario, such large λ_H does not contribute to direct detection of fermion DM. In fact, due to gauge singlet and leptophilic nature of fermion DM there is no tree level direct detection cross section, keeping it safe from Xenon1T bounds. It should also be emphasised that we have no fine-tuning between λ_1 , λ_2 and λ_3 in this scenario, and thus, detectable GW signals at U-DECIGO-corr are naturally produced. However, such leptophilic fermion DM scenario can be tightly constrained by experimental bounds on charged lepton flavour violation as we discuss below.

C. Charged Lepton Flavour Violation

Charged lepton flavour violation (CLFV) arises in the SM at one loop level and remains suppressed by the smallness of neutrino masses, much beyond the current and near future

experimental sensitivities. Therefore, any experimental observation of such processes is definitely a sign of BSM physics, like the one we are studying here. In the present model, this becomes inevitable due to the couplings of new Z_2 odd particles to the SM lepton doublets. The same fields that take part in the one-loop generation of light neutrino mass, can also mediate charged lepton flavour violating processes like $\mu \rightarrow e\gamma$, $\mu \rightarrow 3e$ and $\mu \rightarrow e$ (Ti) conversion. These rare processes have strong current limit as well as good future sensitivity [42]. The present bounds are: $\text{BR}(\mu \rightarrow e\gamma) < 4.2 \times 10^{-13}$ [126], $\text{BR}(\mu \rightarrow 3e) < 1.0 \times 10^{-12}$ [127], $\text{CR}(\mu, \text{Ti} \rightarrow e, \text{Ti}) < 4.3 \times 10^{-12}$ [128]. While the future sensitivity of the first two processes are around one order of magnitude lower than the present branching ratios, the μ to e conversion (Ti) sensitivity is supposed to increase by six order of magnitudes [42] making it a highly promising test to confirm or rule out different TeV scale BSM scenarios.

Since the couplings, masses involved in this process are the same as the ones that generate light neutrino masses and play a role in DM relic abundance, we can no longer choose them arbitrarily. The branching fraction for $\mu \rightarrow e\gamma$ that follows from this one-loop contribution can be written as [43],

$$\text{Br}(\mu \rightarrow e\gamma) = \frac{3(4\pi)^3 \alpha_{\text{em}}}{4G_F^2} |A_D|^2 \text{Br}(\mu \rightarrow e\nu_\mu \bar{\nu}_e). \quad (58)$$

Where α_{em} is the electromagnetic fine structure constant, e is the electromagnetic coupling and G_F is the Fermi constant. A_D is the dipole form factor given by

$$A_D = \sum_{i=1}^3 \frac{Y_{ie}^* Y_{i\mu}}{2(4\pi)^2 m_\pm^2} \left(\frac{1 - 6\xi_i + 3\xi_i^2 + 2\xi_i^3 - 6\xi_i^2 \log \xi_i}{6(1 - \xi_i)^4} \right). \quad (59)$$

Here the parameter ξ_i 's are defined as $\xi_i \equiv M_{N_i}^2/m_\pm^2$. The MEG experiment provides the most stringent upper limit on the branching ratio $\text{Br}(\mu \rightarrow e\gamma) < 4.2 \times 10^{-13}$ [126]. For analytical expressions of other flavour violating processes, please refer to [43]. We have used the `SPheno 3.1` interface [129] in order to implement the flavour constraints into the model. For fermion DM model, the predictions for CLFV processes are shown in figure 6. As can be seen from this figure, all the predicted points lie way below the current experimental bounds. This is due to the fact that fermion singlet DM relic is mainly governed by its coannihilation with inert doublet components and hence even relatively smaller Yukawa couplings can give rise to the correct relic. This was also noted in earlier works [43].

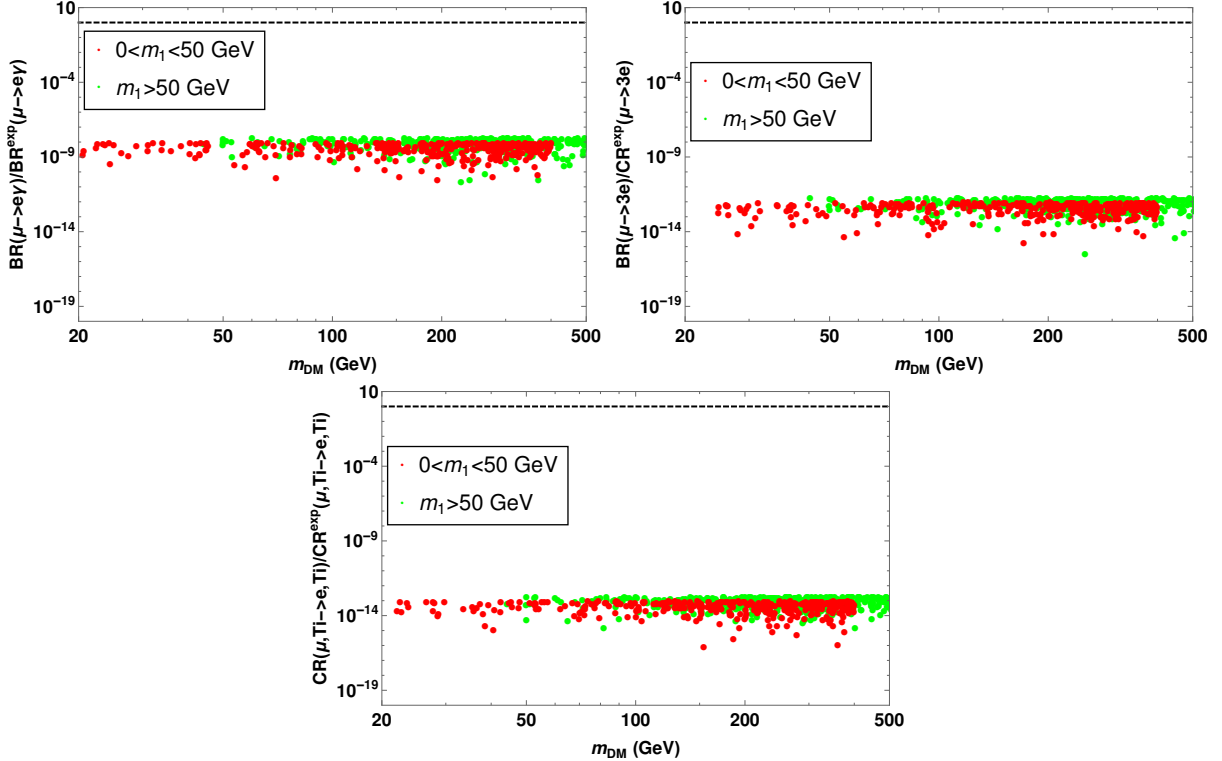


FIG. 6. Predictions for different CLFV processes for fermion DM scenario. All points satisfy the DM relic criteria while the red coloured points satisfy the SFOPT criteria.

VI. CONCLUSION

We have studied the possibility of generating GWs from a strong first-order EWPT in minimal scotogenic model which can be probed at future space based experiments like UDECIGO. While the scalar content of the model is same as that in IDM where the possibility of strong first-order EWPT along with scalar DM has been studied in several earlier works, in the present model we find newer region of parameter space due to the possibility of fermion DM. We also improve earlier studies by appropriate consideration of resummation effects in finite temperature effective potential. Our results in the scalar DM scenario is partially in agreement with earlier works where SFOPT criteria favours a low mass scalar DM which however, remains disfavoured from stringent direct detection bounds from Xenon1T 2018. The parameter space favouring SFOPT can however be enhanced for sub-dominant scalar DM, in agreement with earlier works. More interesting results arise in the fermion DM scenario where the SFOPT favoured parameter space is enlarged primarily due to the fact that mass ordering within the inert scalar doublet components is relaxed in this scenario.

This is contrast with the scalar DM scenario where one of the neutral components was restricted to be the lightest Z_2 odd particle. Also, unlike scalar DM which can satisfy relic in two well defined regions: low mass regime $m_H < 80$ GeV and high mass regime $m_H > 550$ GeV, fermion DM (of thermal WIMP type) relic can be realised for almost any mass, as long as the mass difference between fermion DM and next to lightest Z_2 odd particle is kept small (to enhance coannihilation) and corresponding Yukawa coupling is kept sizeable in agreement with light neutrino masses via Casas-Ibarra parametrisation. The fermion DM scenario therefore, can also be tightly related to light neutrino masses as the same Yukawa couplings go into the light neutrino mass generation at one loop level. While leptophilic fermion DM in this model can also give rise to sizeable charged lepton flavour violation, we find that for the parameter space satisfying SFOPT, DM relic and other relevant bounds, the contribution to charged rare decays remains well below current limits. The possibility of enlarged parameter space in the fermion DM scenario specially having light charged scalars can give rise to interesting signatures at colliders. Such light charged scalars can be produced significantly and can leave interesting signatures like displaced vertex, as discussed recently in [41]. Connection of such strong first-order EWPT to baryogenesis is another interesting possibility which we leave for future studies. While baryogenesis through leptogenesis is already a viable possibility in the minimal scotogenic model [20, 22, 24–28] as mentioned earlier, a GW based probe of this model can indirectly probe the parameter space relevant for successful leptogenesis as well. Similar ways of probing seesaw and leptogenesis have also been proposed recently [130, 131]. However, possible extensions of the scotogenic model in order to implement electroweak baryogenesis may also bring the GW signal within reach of other upcoming experiments like LISA. We leave such detailed studies in connection to baryogenesis to future works.

ACKNOWLEDGMENTS

DB acknowledges the support from Early Career Research Award from the Science and Engineering Research Board (SERB), Department of Science and Technology (DST), Government of India (reference number: ECR/2017/001873). The work of SKK and AD was supported by the NRF of Korea Grants No. 2017K1A3A7A09016430, and No. 2017R1A2B4006338. The work of KF was supported by JSPS Grants-in-Aid for Research

Fellows No. 20J12415. KF was also supported by JSPS and NRF under the Japan-Korea Basic Scientific Cooperation Program and would like to thank participants attending the JSPS and NRF conference for useful comments. DB and KF thank the organisers of *TokyoTech and IIT Guwahati Joint Workshop: Condensed Matter and High-Energy Physics at TokyoTech* during November 11-12, 2019 where part of this work was discussed.

- [1] E. Ma, *Verifiable radiative seesaw mechanism of neutrino mass and dark matter*, *Phys. Rev.* **D73** (2006) 077301, [[hep-ph/0601225](#)].
- [2] **Particle Data Group** Collaboration, M. Tanabashi et al., *Review of Particle Physics*, *Phys. Rev.* **D98** (2018), no. 3 030001.
- [3] P. F. de Salas, D. V. Forero, C. A. Ternes, M. Tortola, and J. W. F. Valle, *Status of neutrino oscillations 2018: 3σ hint for normal mass ordering and improved CP sensitivity*, *Phys. Lett.* **B782** (2018) 633–640, [[arXiv:1708.01186](#)].
- [4] I. Esteban, M. C. Gonzalez-Garcia, A. Hernandez-Cabezudo, M. Maltoni, and T. Schwetz, *Global analysis of three-flavour neutrino oscillations: synergies and tensions in the determination of θ_{23} , δ_{CP} , and the mass ordering*, *JHEP* **01** (2019) 106, [[arXiv:1811.05487](#)].
- [5] **Planck** Collaboration, N. Aghanim et al., *Planck 2018 results. VI. Cosmological parameters*, [arXiv:1807.06209](#).
- [6] M. Cirelli, N. Fornengo, and A. Strumia, *Minimal dark matter*, *Nucl. Phys.* **B753** (2006) 178–194, [[hep-ph/0512090](#)].
- [7] R. Barbieri, L. J. Hall, and V. S. Rychkov, *Improved naturalness with a heavy Higgs: An Alternative road to LHC physics*, *Phys. Rev.* **D74** (2006) 015007, [[hep-ph/0603188](#)].
- [8] E. Ma, *Common origin of neutrino mass, dark matter, and baryogenesis*, *Mod. Phys. Lett.* **A21** (2006) 1777–1782, [[hep-ph/0605180](#)].
- [9] L. Lopez Honorez, E. Nezri, J. F. Oliver, and M. H. G. Tytgat, *The Inert Doublet Model: An Archetype for Dark Matter*, *JCAP* **0702** (2007) 028, [[hep-ph/0612275](#)].
- [10] T. Hambye, F. S. Ling, L. Lopez Honorez, and J. Rocher, *Scalar Multiplet Dark Matter*, *JHEP* **07** (2009) 090, [[arXiv:0903.4010](#)]. [Erratum: JHEP05,066(2010)].

- [11] E. M. Dolle and S. Su, *The Inert Dark Matter*, *Phys. Rev.* **D80** (2009) 055012, [[arXiv:0906.1609](#)].
- [12] L. Lopez Honorez and C. E. Yaguna, *The inert doublet model of dark matter revisited*, *JHEP* **09** (2010) 046, [[arXiv:1003.3125](#)].
- [13] L. Lopez Honorez and C. E. Yaguna, *A new viable region of the inert doublet model*, *JCAP* **1101** (2011) 002, [[arXiv:1011.1411](#)].
- [14] M. Gustafsson, S. Rydbeck, L. Lopez-Honorez, and E. Lundstrom, *Status of the Inert Doublet Model and the Role of multileptons at the LHC*, *Phys. Rev.* **D86** (2012) 075019, [[arXiv:1206.6316](#)].
- [15] A. Goudelis, B. Herrmann, and O. Stal, *Dark matter in the Inert Doublet Model after the discovery of a Higgs-like boson at the LHC*, *JHEP* **09** (2013) 106, [[arXiv:1303.3010](#)].
- [16] A. Arhrib, Y.-L. S. Tsai, Q. Yuan, and T.-C. Yuan, *An Updated Analysis of Inert Higgs Doublet Model in light of the Recent Results from LUX, PLANCK, AMS-02 and LHC*, *JCAP* **1406** (2014) 030, [[arXiv:1310.0358](#)].
- [17] A. Dasgupta and D. Borah, *Scalar Dark Matter with Type II Seesaw*, *Nucl. Phys.* **B889** (2014) 637–649, [[arXiv:1404.5261](#)].
- [18] M. A. Diaz, B. Koch, and S. Urrutia-Quiroga, *Constraints to Dark Matter from Inert Higgs Doublet Model*, *Adv. High Energy Phys.* **2016** (2016) 8278375, [[arXiv:1511.04429](#)].
- [19] D. Borah and A. Gupta, *New viable region of an inert Higgs doublet dark matter model with scotogenic extension*, *Phys. Rev.* **D96** (2017), no. 11 115012, [[arXiv:1706.05034](#)].
- [20] D. Borah, P. S. B. Dev, and A. Kumar, *TeV scale leptogenesis, inflaton dark matter and neutrino mass in a scotogenic model*, *Phys. Rev.* **D99** (2019), no. 5 055012, [[arXiv:1810.03645](#)].
- [21] A. Ahriche, A. Jueid, and S. Nasri, *Radiative neutrino mass and Majorana dark matter within an inert Higgs doublet model*, *Phys. Rev.* **D97** (2018), no. 9 095012, [[arXiv:1710.03824](#)].
- [22] D. Mahanta and D. Borah, *Fermion dark matter with N_2 leptogenesis in minimal scotogenic model*, *JCAP* **1911** (2019), no. 11 021, [[arXiv:1906.03577](#)].
- [23] S. Davidson, E. Nardi, and Y. Nir, *Leptogenesis*, *Phys. Rept.* **466** (2008) 105–177, [[arXiv:0802.2962](#)].

- [24] T. Hugle, M. Platscher, and K. Schmitz, *Low-Scale Leptogenesis in the Scotogenic Neutrino Mass Model*, *Phys. Rev.* **D98** (2018), no. 2 023020, [[arXiv:1804.09660](#)].
- [25] W.-C. Huang, H. Pas, and S. Zeissner, *Scalar Dark Matter, GUT baryogenesis and Radiative neutrino mass*, *Phys. Rev.* **D98** (2018), no. 7 075024, [[arXiv:1806.08204](#)].
- [26] S. Baumholzer, V. Brdar, and P. Schwaller, *The New ν MSM ($\nu\nu$ MSM): Radiative Neutrino Masses, keV-Scale Dark Matter and Viable Leptogenesis with sub-TeV New Physics*, *JHEP* **08** (2018) 067, [[arXiv:1806.06864](#)].
- [27] D. Borah, A. Dasgupta, and S. K. Kang, *Leptogenesis from Dark Matter Annihilations in Scotogenic Model*, [arXiv:1806.04689](#).
- [28] D. Mahanta and D. Borah, *TeV Scale Leptogenesis with Dark Matter in Non-standard Cosmology*, [arXiv:1912.09726](#).
- [29] G. Arcadi, M. Dutra, P. Ghosh, M. Lindner, Y. Mambrini, M. Pierre, S. Profumo, and F. S. Queiroz, *The Waning of the WIMP? A Review of Models, Searches, and Constraints*, [arXiv:1703.07364](#).
- [30] **LUX** Collaboration, D. S. Akerib et al., *Results from a search for dark matter in the complete LUX exposure*, *Phys. Rev. Lett.* **118** (2017), no. 2 021303, [[arXiv:1608.07648](#)].
- [31] **PandaX-II** Collaboration, A. Tan et al., *Dark Matter Results from First 98.7 Days of Data from the PandaX-II Experiment*, *Phys. Rev. Lett.* **117** (2016), no. 12 121303, [[arXiv:1607.07400](#)].
- [32] **PandaX-II** Collaboration, X. Cui et al., *Dark Matter Results From 54-Ton-Day Exposure of PandaX-II Experiment*, *Phys. Rev. Lett.* **119** (2017), no. 18 181302, [[arXiv:1708.06917](#)].
- [33] **XENON** Collaboration, E. Aprile et al., *First Dark Matter Search Results from the XENON1T Experiment*, *Phys. Rev. Lett.* **119** (2017), no. 18 181301, [[arXiv:1705.06655](#)].
- [34] E. Aprile et al., *Dark Matter Search Results from a One Tonne \times Year Exposure of XENON1T*, [arXiv:1805.12562](#).
- [35] S. Baumholzer, V. Brdar, P. Schwaller, and A. Segner, *Shining Light on the Scotogenic Model: Interplay of Colliders, Cosmology and Astrophysics*, [arXiv:1912.08215](#).
- [36] X. Miao, S. Su, and B. Thomas, *Trilepton Signals in the Inert Doublet Model*, *Phys. Rev.* **D82** (2010) 035009, [[arXiv:1005.0090](#)].
- [37] A. Datta, N. Ganguly, N. Khan, and S. Rakshit, *Exploring collider signatures of the inert Higgs doublet model*, *Phys. Rev.* **D95** (2017), no. 1 015017, [[arXiv:1610.00648](#)].

- [38] P. Poulou, S. Sahoo, and K. Sridhar, *Exploring the Inert Doublet Model through the dijet plus missing transverse energy channel at the LHC*, *Phys. Lett.* **B765** (2017) 300–306, [[arXiv:1604.03045](#)].
- [39] A. Belyaev, G. Cacciapaglia, I. P. Ivanov, F. Rojas, and M. Thomas, *Anatomy of the Inert Two Higgs Doublet Model in the light of the LHC and non-LHC Dark Matter Searches*, [arXiv:1612.00511](#).
- [40] A. Belyaev, T. R. Fernandez Perez Tomei, P. G. Mercadante, C. S. Moon, S. Moretti, S. F. Novaes, L. Panizzi, F. Rojas, and M. Thomas, *Advancing LHC probes of dark matter from the inert two-Higgs-doublet model with the monojet signal*, *Phys. Rev.* **D99** (2019), no. 1 015011, [[arXiv:1809.00933](#)].
- [41] D. Borah, D. Nanda, N. Narendra, and N. Sahu, *Right-handed neutrino dark matter with radiative neutrino mass in gauged $B - L$ model*, *Nucl. Phys.* **B950** (2020) 114841, [[arXiv:1810.12920](#)].
- [42] T. Toma and A. Vicente, *Lepton Flavor Violation in the Scotogenic Model*, *JHEP* **01** (2014) 160, [[arXiv:1312.2840](#)].
- [43] A. Vicente and C. E. Yaguna, *Probing the scotogenic model with lepton flavor violating processes*, *JHEP* **02** (2015) 144, [[arXiv:1412.2545](#)].
- [44] **LISA** Collaboration, W. M. Folkner, *The LISA mission design*, *AIP Conf. Proc.* **456** (1998), no. 1 11–16.
- [45] **LISA** Collaboration, P. Amaro-Seoane et al., *Laser Interferometer Space Antenna*, [arXiv:1702.00786](#).
- [46] **LISA Cosmology Working Group** Collaboration, E. Belgacem et al., *Testing modified gravity at cosmological distances with LISA standard sirens*, *JCAP* **1907** (2019), no. 07 024, [[arXiv:1906.01593](#)].
- [47] **LISA Pathfinder** Collaboration, M. Armano et al., *Novel methods to measure the gravitational constant in space*, *Phys. Rev.* **D100** (2019), no. 6 062003.
- [48] C. Caprini et al., *Science with the space-based interferometer eLISA. II: Gravitational waves from cosmological phase transitions*, *JCAP* **04** (2016) 001, [[arXiv:1512.06239](#)].
- [49] C. Caprini et al., *Detecting gravitational waves from cosmological phase transitions with LISA: an update*, *JCAP* **03** (2020) 024, [[arXiv:1910.13125](#)].

- [50] H. Kudoh, A. Taruya, T. Hiramatsu, and Y. Himemoto, *Detecting a gravitational-wave background with next-generation space interferometers*, *Phys. Rev.* **D73** (2006) 064006, [[gr-qc/0511145](#)].
- [51] S. Sato et al., *The status of DECIGO*, *J. Phys. Conf. Ser.* **840** (2017), no. 1 012010.
- [52] T. Alanne, T. Hügler, M. Platscher, and K. Schmitz, *A fresh look at the gravitational-wave signal from cosmological phase transitions*, *JHEP* **03** (2020) 004, [[arXiv:1909.11356](#)].
- [53] K. Schmitz, *New Sensitivity Curves for Gravitational-Wave Experiments*, [arXiv:2002.04615](#).
- [54] M. S. Turner and F. Wilczek, *Relic gravitational waves and extended inflation*, *Phys. Rev. Lett.* **65** (1990) 3080–3083.
- [55] A. Kosowsky, M. S. Turner, and R. Watkins, *Gravitational radiation from colliding vacuum bubbles*, *Phys. Rev.* **D45** (1992) 4514–4535.
- [56] A. Kosowsky, M. S. Turner, and R. Watkins, *Gravitational waves from first order cosmological phase transitions*, *Phys. Rev. Lett.* **69** (1992) 2026–2029.
- [57] A. Kosowsky and M. S. Turner, *Gravitational radiation from colliding vacuum bubbles: envelope approximation to many bubble collisions*, *Phys. Rev.* **D47** (1993) 4372–4391, [[astro-ph/9211004](#)].
- [58] M. S. Turner, E. J. Weinberg, and L. M. Widrow, *Bubble nucleation in first order inflation and other cosmological phase transitions*, *Phys. Rev.* **D46** (1992) 2384–2403.
- [59] M. Hindmarsh, S. J. Huber, K. Rummukainen, and D. J. Weir, *Gravitational waves from the sound of a first order phase transition*, *Phys. Rev. Lett.* **112** (2014) 041301, [[arXiv:1304.2433](#)].
- [60] J. T. Giblin and J. B. Mertens, *Gravitational radiation from first-order phase transitions in the presence of a fluid*, *Phys. Rev.* **D90** (2014), no. 2 023532, [[arXiv:1405.4005](#)].
- [61] M. Hindmarsh, S. J. Huber, K. Rummukainen, and D. J. Weir, *Numerical simulations of acoustically generated gravitational waves at a first order phase transition*, *Phys. Rev.* **D92** (2015), no. 12 123009, [[arXiv:1504.03291](#)].
- [62] M. Hindmarsh, S. J. Huber, K. Rummukainen, and D. J. Weir, *Shape of the acoustic gravitational wave power spectrum from a first order phase transition*, *Phys. Rev.* **D96** (2017), no. 10 103520, [[arXiv:1704.05871](#)].

- [63] M. Kamionkowski, A. Kosowsky, and M. S. Turner, *Gravitational radiation from first order phase transitions*, *Phys. Rev.* **D49** (1994) 2837–2851, [[astro-ph/9310044](#)].
- [64] A. Kosowsky, A. Mack, and T. Kahniashvili, *Gravitational radiation from cosmological turbulence*, *Phys. Rev.* **D66** (2002) 024030, [[astro-ph/0111483](#)].
- [65] C. Caprini and R. Durrer, *Gravitational waves from stochastic relativistic sources: Primordial turbulence and magnetic fields*, *Phys. Rev.* **D74** (2006) 063521, [[astro-ph/0603476](#)].
- [66] G. Gogoberidze, T. Kahniashvili, and A. Kosowsky, *The Spectrum of Gravitational Radiation from Primordial Turbulence*, *Phys. Rev.* **D76** (2007) 083002, [[arXiv:0705.1733](#)].
- [67] C. Caprini, R. Durrer, and G. Servant, *The stochastic gravitational wave background from turbulence and magnetic fields generated by a first-order phase transition*, *JCAP* **0912** (2009) 024, [[arXiv:0909.0622](#)].
- [68] P. Niksa, M. Schlexer, and G. Sigl, *Gravitational Waves produced by Compressible MHD Turbulence from Cosmological Phase Transitions*, *Class. Quant. Grav.* **35** (2018), no. 14 144001, [[arXiv:1803.02271](#)].
- [69] A. Mazumdar and G. White, *Review of cosmic phase transitions: their significance and experimental signatures*, *Rept. Prog. Phys.* **82** (2019), no. 7 076901, [[arXiv:1811.01948](#)].
- [70] F. Csikor, Z. Fodor, and J. Heitger, *Endpoint of the hot electroweak phase transition*, *Phys. Rev. Lett.* **82** (1999) 21–24, [[hep-ph/9809291](#)].
- [71] K. Rummukainen, M. Tsypin, K. Kajantie, M. Laine, and M. E. Shaposhnikov, *The Universality class of the electroweak theory*, *Nucl. Phys.* **B532** (1998) 283–314, [[hep-lat/9805013](#)].
- [72] T. A. Chowdhury, M. Nemevsek, G. Senjanovic, and Y. Zhang, *Dark Matter as the Trigger of Strong Electroweak Phase Transition*, *JCAP* **1202** (2012) 029, [[arXiv:1110.5334](#)].
- [73] D. Borah and J. M. Cline, *Inert Doublet Dark Matter with Strong Electroweak Phase Transition*, *Phys. Rev.* **D86** (2012) 055001, [[arXiv:1204.4722](#)].
- [74] G. Gil, P. Chankowski, and M. Krawczyk, *Inert Dark Matter and Strong Electroweak Phase Transition*, *Phys. Lett.* **B717** (2012) 396–402, [[arXiv:1207.0084](#)].
- [75] J. M. Cline and K. Kainulainen, *Improved Electroweak Phase Transition with Subdominant Inert Doublet Dark Matter*, *Phys. Rev.* **D87** (2013), no. 7 071701, [[arXiv:1302.2614](#)].

- [76] N. Blinov, S. Profumo, and T. Stefaniak, *The Electroweak Phase Transition in the Inert Doublet Model*, *JCAP* **1507** (2015), no. 07 028, [[arXiv:1504.05949](#)].
- [77] F. P. Huang and J.-H. Yu, *Exploring inert dark matter blind spots with gravitational wave signatures*, *Phys. Rev.* **D98** (2018), no. 9 095022, [[arXiv:1704.04201](#)].
- [78] X. Liu and L. Bian, *Dark matter and electroweak phase transition in the mixed scalar dark matter model*, *Phys. Rev.* **D97** (2018), no. 5 055028, [[arXiv:1706.06042](#)].
- [79] K. Hashino, R. Jinno, M. Kakizaki, S. Kanemura, T. Takahashi, and M. Takimoto, *Selecting models of first-order phase transitions using the synergy between collider and gravitational-wave experiments*, *Phys. Rev.* **D99** (2019), no. 7 075011, [[arXiv:1809.04994](#)].
- [80] A. Merle and M. Platscher, *Running of radiative neutrino masses: the scotogenic model ? revisited*, *JHEP* **11** (2015) 148, [[arXiv:1507.06314](#)].
- [81] J. A. Casas and A. Ibarra, *Oscillating neutrinos and muon $\rightarrow e, \gamma$* , *Nucl. Phys.* **B618** (2001) 171–204, [[hep-ph/0103065](#)].
- [82] E. Lundstrom, M. Gustafsson, and J. Edsjo, *The Inert Doublet Model and LEP II Limits*, *Phys. Rev.* **D79** (2009) 035013, [[arXiv:0810.3924](#)].
- [83] **ATLAS** Collaboration, M. Aaboud et al., *Combination of searches for invisible Higgs boson decays with the ATLAS experiment*, *Phys. Rev. Lett.* **122** (2019), no. 23 231801, [[arXiv:1904.05105](#)].
- [84] D. Borah and A. Dasgupta, *Left?right symmetric models with a mixture of keV?TeV dark matter*, *J. Phys.* **G46** (2019), no. 10 105004, [[arXiv:1710.06170](#)].
- [85] M. Hashemi and S. Najjari, *Observability of Inert Scalars at the LHC*, [arXiv:1611.07827](#).
- [86] D. Borah, S. Sadhukhan, and S. Sahoo, *Lepton Portal Limit of Inert Higgs Doublet Dark Matter with Radiative Neutrino Mass*, [arXiv:1703.08674](#).
- [87] M. Sher, *Electroweak Higgs Potentials and Vacuum Stability*, *Phys. Rept.* **179** (1989) 273–418.
- [88] G. C. Branco, P. M. Ferreira, L. Lavoura, M. N. Rebelo, M. Sher, and J. P. Silva, *Theory and phenomenology of two-Higgs-doublet models*, *Phys. Rept.* **516** (2012) 1–102, [[arXiv:1106.0034](#)].
- [89] D. Dercks and T. Robens, *Constraining the Inert Doublet Model using Vector Boson Fusion*, *Eur. Phys. J.* **C79** (2019), no. 11 924, [[arXiv:1812.07913](#)].

- [90] I. F. Ginzburg and I. P. Ivanov, *Tree-level unitarity constraints in the most general 2HDM*, *Phys. Rev.* **D72** (2005) 115010, [[hep-ph/0508020](#)].
- [91] M. Aoki, S. Kanemura, M. Kikuchi, and K. Yagyu, *Renormalization of the Higgs Sector in the Triplet Model*, *Phys. Lett.* **B714** (2012) 279–285, [[arXiv:1204.1951](#)].
- [92] L. Dolan and R. Jackiw, *Symmetry Behavior at Finite Temperature*, *Phys. Rev.* **D9** (1974) 3320–3341.
- [93] M. Quiros, *Finite temperature field theory and phase transitions*, in *Proceedings, Summer School in High-energy physics and cosmology: Trieste, Italy, June 29-July 17, 1998*, pp. 187–259, 1999. [hep-ph/9901312](#).
- [94] C. Wainwright, S. Profumo, and M. J. Ramsey-Musolf, *Gravity Waves from a Cosmological Phase Transition: Gauge Artifacts and Daisy Resummations*, *Phys. Rev.* **D84** (2011) 023521, [[arXiv:1104.5487](#)].
- [95] C. L. Wainwright, S. Profumo, and M. J. Ramsey-Musolf, *Phase Transitions and Gauge Artifacts in an Abelian Higgs Plus Singlet Model*, *Phys. Rev.* **D86** (2012) 083537, [[arXiv:1204.5464](#)].
- [96] S. R. Coleman and E. J. Weinberg, *Radiative Corrections as the Origin of Spontaneous Symmetry Breaking*, *Phys. Rev.* **D7** (1973) 1888–1910.
- [97] P. Fendley, *The Effective Potential and the Coupling Constant at High Temperature*, *Phys. Lett.* **B196** (1987) 175–180.
- [98] R. R. Parwani, *Resummation in a hot scalar field theory*, *Phys. Rev.* **D45** (1992) 4695, [[hep-ph/9204216](#)]. [Erratum: *Phys. Rev.*D48,5965(1993)].
- [99] P. B. Arnold and O. Espinosa, *The Effective potential and first order phase transitions: Beyond leading-order*, *Phys. Rev.* **D47** (1993) 3546, [[hep-ph/9212235](#)]. [Erratum: *Phys. Rev.*D50,6662(1994)].
- [100] P. Basler, M. Krause, M. Muhlleitner, J. Wittbrodt, and A. Wlotzka, *Strong First Order Electroweak Phase Transition in the CP-Conserving 2HDM Revisited*, *JHEP* **02** (2017) 121, [[arXiv:1612.04086](#)].
- [101] C. L. Wainwright, *CosmoTransitions: Computing Cosmological Phase Transition Temperatures and Bubble Profiles with Multiple Fields*, *Comput. Phys. Commun.* **183** (2012) 2006–2013, [[arXiv:1109.4189](#)].

- [102] A. D. Linde, *Infrared Problem in Thermodynamics of the Yang-Mills Gas*, *Phys. Lett.* **96B** (1980) 289–292.
- [103] M. E. Carrington, *The Effective potential at finite temperature in the Standard Model*, *Phys. Rev.* **D45** (1992) 2933–2944.
- [104] J. I. Kapusta and C. Gale, *Finite-temperature field theory: Principles and applications*. Cambridge Monographs on Mathematical Physics. Cambridge University Press, 2011.
- [105] A. D. Linde, *Fate of the False Vacuum at Finite Temperature: Theory and Applications*, *Phys. Lett.* **100B** (1981) 37–40.
- [106] F. Giese, T. Konstandin, and J. van de Vis, *Model-independent energy budget of cosmological first-order phase transitions*, [arXiv:2004.06995](#).
- [107] D. Bodeker and G. D. Moore, *Electroweak Bubble Wall Speed Limit*, *JCAP* **1705** (2017), no. 05 025, [[arXiv:1703.08215](#)].
- [108] J. Ellis, M. Lewicki, J. M. No, and V. Vaskonen, *Gravitational wave energy budget in strongly supercooled phase transitions*, *JCAP* **1906** (2019), no. 06 024, [[arXiv:1903.09642](#)].
- [109] P. Binetruy, A. Bohe, C. Caprini, and J.-F. Dufaux, *Cosmological Backgrounds of Gravitational Waves and eLISA/NGO: Phase Transitions, Cosmic Strings and Other Sources*, *JCAP* **1206** (2012) 027, [[arXiv:1201.0983](#)].
- [110] J. Ellis, M. Lewicki, and J. M. No, *On the Maximal Strength of a First-Order Electroweak Phase Transition and its Gravitational Wave Signal*, [arXiv:1809.08242](#). [*JCAP*1904,003(2019)].
- [111] D. Cutting, M. Hindmarsh, and D. J. Weir, *Vorticity, kinetic energy, and suppressed gravitational wave production in strong first order phase transitions*, [arXiv:1906.00480](#).
- [112] J. Ellis, M. Lewicki, and J. M. No, *Gravitational waves from first-order cosmological phase transitions: lifetime of the sound wave source*, [arXiv:2003.07360](#).
- [113] P. J. Steinhardt, *Relativistic Detonation Waves and Bubble Growth in False Vacuum Decay*, *Phys. Rev.* **D25** (1982) 2074.
- [114] S. J. Huber and M. Sopena, *An efficient approach to electroweak bubble velocities*, [arXiv:1302.1044](#).
- [115] L. Leitao and A. Megevand, *Hydrodynamics of phase transition fronts and the speed of sound in the plasma*, *Nucl. Phys.* **B891** (2015) 159–199, [[arXiv:1410.3875](#)].

- [116] G. C. Dorsch, S. J. Huber, and T. Konstandin, *Bubble wall velocities in the Standard Model and beyond*, *JCAP* **1812** (2018), no. 12 034, [[arXiv:1809.04907](#)].
- [117] J. M. Cline and K. Kainulainen, *Electroweak baryogenesis at high wall velocities*, [arXiv:2001.00568](#).
- [118] J. R. Espinosa, T. Konstandin, J. M. No, and G. Servant, *Energy Budget of Cosmological First-order Phase Transitions*, *JCAP* **06** (2010) 028, [[arXiv:1004.4187](#)].
- [119] P. Gondolo and G. Gelmini, *Cosmic abundances of stable particles: Improved analysis*, *Nucl. Phys.* **B360** (1991) 145–179.
- [120] K. Griest and D. Seckel, *Three exceptions in the calculation of relic abundances*, *Phys. Rev.* **D43** (1991) 3191–3203.
- [121] G. Belanger, F. Boudjema, A. Pukhov, and A. Semenov, *micrOMEGAs 3: A program for calculating dark matter observables*, *Comput. Phys. Commun.* **185** (2014) 960–985, [[arXiv:1305.0237](#)].
- [122] A. Klein et al., *Science with the space-based interferometer eLISA: Supermassive black hole binaries*, *Phys. Rev. D* **93** (2016), no. 2 024003, [[arXiv:1511.05581](#)].
- [123] K. Yagi and N. Seto, *Detector configuration of DECIGO/BBO and identification of cosmological neutron-star binaries*, *Phys. Rev. D* **83** (2011) 044011, [[arXiv:1101.3940](#)].
[Erratum: *Phys.Rev.D* 95, 109901 (2017)].
- [124] M. Punturo et al., *The Einstein Telescope: A third-generation gravitational wave observatory*, *Class. Quant. Grav.* **27** (2010) 194002.
- [125] S. Hild et al., *Sensitivity Studies for Third-Generation Gravitational Wave Observatories*, *Class. Quant. Grav.* **28** (2011) 094013, [[arXiv:1012.0908](#)].
- [126] **MEG** Collaboration, A. M. Baldini et al., *Search for the lepton flavour violating decay $\mu^+ \rightarrow e^+ \gamma$ with the full dataset of the MEG experiment*, *Eur. Phys. J.* **C76** (2016), no. 8 434, [[arXiv:1605.05081](#)].
- [127] **SINDRUM** Collaboration, U. Bellgardt et al., *Search for the Decay $\mu^+ \rightarrow e^+ e^+ e^-$* , *Nucl. Phys.* **B299** (1988) 1–6.
- [128] **SINDRUM II** Collaboration, C. Dohmen et al., *Test of lepton flavor conservation in $\mu^+ \rightarrow e^+ e^-$ conversion on titanium*, *Phys. Lett.* **B317** (1993) 631–636.
- [129] W. Porod and F. Staub, *SPheno 3.1: Extensions including flavour, CP-phases and models beyond the MSSM*, *Comput. Phys. Commun.* **183** (2012) 2458–2469, [[arXiv:1104.1573](#)].

- [130] J. A. Dror, T. Hiramatsu, K. Kohri, H. Murayama, and G. White, *Testing the Seesaw Mechanism and Leptogenesis with Gravitational Waves*, *Phys. Rev. Lett.* **124** (2020), no. 4 041804, [[arXiv:1908.03227](#)].
- [131] S. Blasi, V. Brdar, and K. Schmitz, *Fingerprint of Low-Scale Leptogenesis in the Primordial Gravitational-Wave Spectrum*, [arXiv:2004.02889](#).